Marine and Petroleum Geology 142 (2022) 105730

Contents lists available at ScienceDirect

Marine and Petroleum Geology

journal homepage: www.elsevier.com/locate/marpetgeo

Subtle reservoirs and implications for hydrocarbon exploration in terrestrial lacustrine fan-delta deposits: Insights from the Triassic Baikouquan Formation, Mahu Sag, Junggar Basin, western China

Zhichao Yu [a], Zhizhang Wang [a,*], Jie Wang [b], Ziyan Li [a]

[a] College of Geosciences, China University of Petroleum, Beijing, 102249, China
[b] CNOOC China Limited, Shenzhen Branch, Shenzhen, Guangdong, 518064, China

ARTICLE INFO

Keywords:
Lacustrine fan delta
Sequence stratigraphy
Sedimentary basin evolution
Subtle reservoir
Hydrocarbon reservoir models

ABSTRACT

Petroleum reserves are abundant in the large-scale lacustrine fan delta reservoirs containing mixed oil in the Baikouquan Formation (MA131 Block, Junggar Basin). However, detecting such subtle reservoirs in the lacustrine foreland basins is challenging. High-resolution sequence stratigraphy, sedimentary basin evolution, and reservoir models are established by integrating the results obtained via wireline log data, cores, thin sections, and seismic data. A fifth-order sequence stratigraphic framework for the Baikouquan Formation is established, which enables the reconstruction of the sedimentary basin evolution and further detailing of the reservoir model, such that the correlation to multistage progradation and retrogradation of the fan delta complex can be determined. The study of core samples led to the identification of eight microfacies, of which sandy debris flows and distributary channels dominate approximately 80% of the depositional system. Stratal slices enable the characterization of the northern Xiazijie and eastern Madong fan-delta systems. The northern Xiazijie fan delta is widely distributed throughout sequences SSQ1–SSQ6, whereas the Xiazijie fan delta underwent, in general, gradual retrogradation during the formation of sequences SSQ6 and SSQ7. The eastern Madong gravity flow fan-delta system only developed during the formation of sequences SSQ1–SSQ5 at the location of an abrupt slope break. There are nine categories of reservoir models in the study area based on the source rocks, faults, and reservoirs. Geomorphology and climate are crucial in controlling the sedimentary infill. Deep faults and an unconformity between the Permian and the Triassic of the Mahu Sag played a decisive role in controlling the hydrocarbon migration pathways. The faults, source rocks, and microfacies together exert considerable control on hydrocarbon accumulation. Within the nearshore fan-delta front, variable reservoir quality can be observed. Crucial factors in improving reservoir quality are fine-grain size and relatively low clay content. This study may facilitate subtle reservoir characterization in other basins.

1. Introduction

Hydrocarbon exploration has been primarily focusing on structural traps using either paleogeomorphic maps or surface outcrop data. With decreasing probability of the discovery of large oil and gas reservoirs, seeking subtle oil and gas resources has considerably progressed (Amy, 2019; Warnecke and Aigner, 2019). The concept of a subtle trap was first proposed by Carll (1880), which was used to represent stratigraphic, unconformity, and paleogeomorphic traps that are different from structural traps. With the advancement of exploration, development, and theoretical research of subtle reservoirs, there have been substantial breakthroughs in new theories and technologies, such as sequence stratigraphy, lithofacies paleogeography, paleogeomorphology analysis, reservoir-forming dynamics, seismic attribute analysis technology, and high-resolution seismic inversion technology (Ehman et al., 2021; Anyiam and Uzuegbu, 2020; Xian et al., 2018). This helps in demonstrating the reservoir-forming mechanism of subtle reservoirs and providing strong technical support for their broad exploration and exploitation strategy.

Most continental basins in China are characterized by variable lithofacies, particularly a small reservoir scale and complex reservoir-forming mechanism (Dai et al., 2021; Tian et al., 2022). Recently, as the oil fields gradually enter a medium-to-high exploration stage, the exploration target has transformed from the original large structural

* Corresponding author.
E-mail address: wang_zhizhang@126.com (Z. Wang).

https://doi.org/10.1016/j.marpetgeo.2022.105730
Received 9 March 2022; Received in revised form 30 April 2022; Accepted 5 May 2022
Available online 10 May 2022

reservoir into a subtle reservoir controlled by factors such as lithology, stratum, and low-amplitude structure (Yu and Wang, 2021; Song et al., 2020). Statistically, the proportion of proven reserves of subtle reservoirs of total discovered reserves in China's petroliferous basins has exhibited a yearly increase, such as the Junggar Basin and Ordos Basin, with 70% in the east and 85% in the west (Li et al., 2017).

Subtle petroleum traps have become an important target for exploration in the Junggar Basin, western China, where the large lacustrine fan delta of the Baikouquan Formation is found in the slope belt of the Mahu Sag, including the Xiazijie, Huangyangquan, and Karamay fans (Zhu et al., 2019; ZHAO et al., 2019). Contrary to the fan delta developed in the marine environment, the lacustrine fan delta is poorly influenced by waves and tides, well preserving its internal sedimentary characteristics and forming a large-scale lithological reservoir. Thus far, a great quantity of hydrocarbon has been discovered and extracted from the Triassic Baikouquan Formation in the fan-delta complex (Xiao et al., 2021; Tang et al., 2021). However, the reservoir is characterized by a regionally mixed source of crude oil, various reservoir types, and complex hydrocarbon accumulation mechanism, restricting subtle reservoir development. Few studies have focused on the applications of seismic data to study the sedimentary-filling evolution in a fifth-order sequence framework. In general, hydrocarbon reservoirs vary in different regions and stages as hydrocarbon enrichment is dominated by a combination of different source rocks, reservoir-seal assemblages, traps, and their temporal as well as spatial distributions. In this study, a series of hydrocarbon reservoir models were proposed to better clarify the hydrocarbon enrichment law in such lacustrine fan delta deposits. We integrated the results obtained from wireline logs, core samples, three-dimensional (3D) seismic cube, formation testing data, and production data for thoroughly demonstrating the sedimentary evolution under the fifth-order stratigraphic sequence framework and the formation of the hydrocarbon reservoirs in the strata. This study aims to

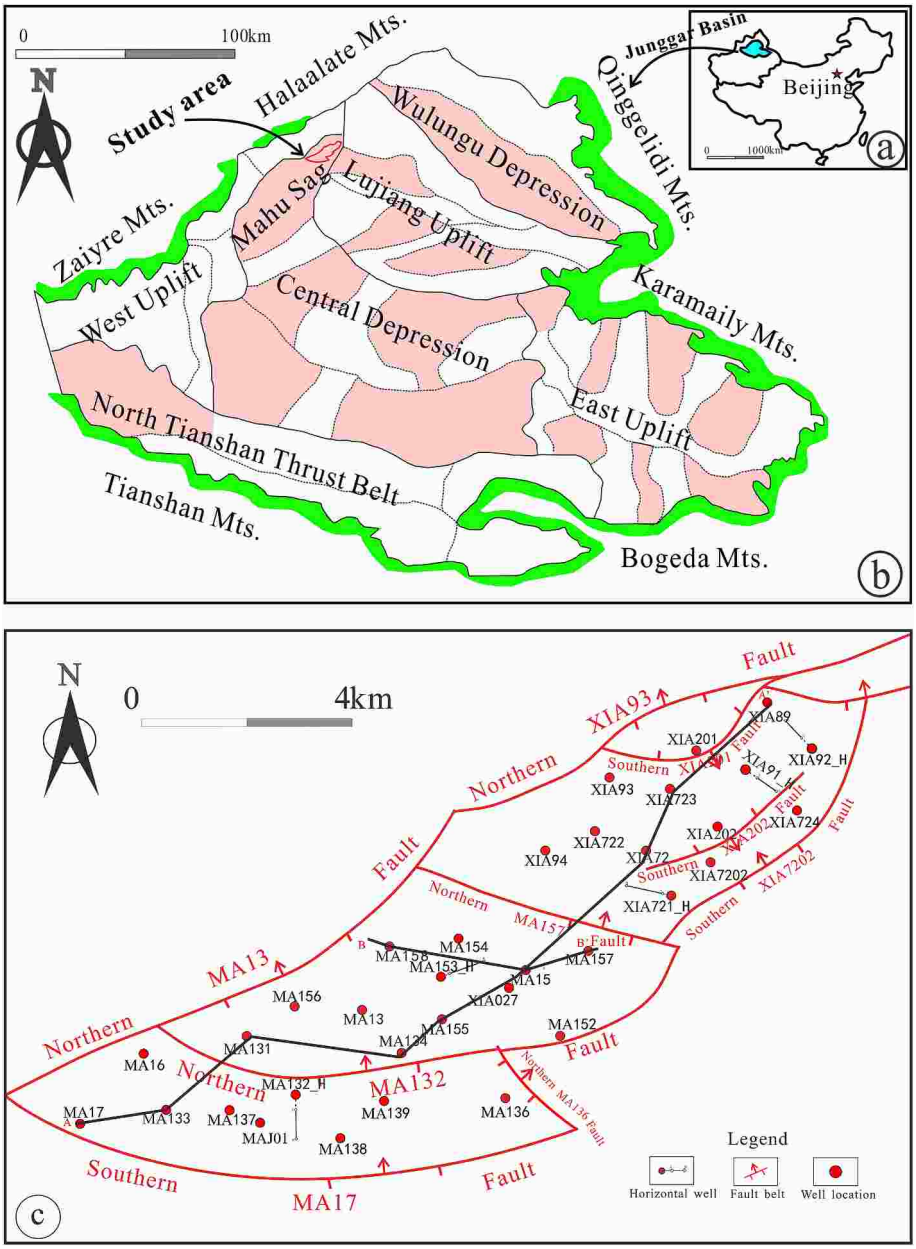

Fig. 1. Tectonic maps showing the locations of (a) the Junggar Basin and (b) the Mahu Sag and major tectonic units of the Junggar Basin. The red polygon represents the study region. (c) The well location map of the MA131 well block; the cross section in Figs. 3 and 10 (outlined by the black line) and secondary thrust faults are shown. (For interpretation of the references to color in this figure legend, the reader is referred to the Web version of this article.)

construct a high-resolution stratigraphic sequence framework; to depict the sedimentary evolution of the fan delta deposits; to summarize the hydrocarbon models; and to discuss the depositional model, hydrocarbon accumulation in the study area, and implications for petroleum exploration.

2. Geological setting

The Junggar Basin (total area ~13 × 10^4 km^2) is a large continental basin known to have undergone the Late Carboniferous–Quaternary tectonic events on a regional scale in Northwest China (Fig. 1a). The compression and nappe between plates caused the formation of the continental foreland basin along the northwestern edge of the basin in the Early–Middle Permian. During the Late Permian, the basin underwent a large-scale tectonic movement again and the foreland basin gradually evolved into a depression basin. Subsequent tectonic events considerably weakened and the stratum subsided intermittently, forming the present-day stratigraphic distribution pattern. The basin is surrounded by the Paleozoic mountains, including northwestern Hala'alat as well as Zhayier, northeastern Kelameili, southeastern Bogeda, and southwestern Yilinheibiergen (Fig. 1b).

The Mahu Sag (100-km long; 50-km wide) is located along the northern edge of the basin, flanked to the west by the Kebai and Wuxia fault zones and to the east by the Dabasong and Xiayan uplifts (Fig. 1b). It is a secondary structural unit belonging to the central depression, covering an area of ~6800 km^2. The research region MA131 well block is seated on the clival area of the northern Mahu Sag and is dominated by the Xiazijie fan-delta complex. This region is a monocline gently dipping to the south (Fig. 1c). Prefan-delta facies, fan-delta front facies, and fan-delta plain facies had successively developed from west to east (Lu et al., 2019). Nose convex, groove, and platform structures have developed locally, and two groups of 10–40 m reverse faults have developed in the study area (Liang et al., 2020). From northeast to southwest, the MA131 well block can be divided into three fault blocks: XIA72, MA131, and MA133 fault blocks (Fig. 1c).

The Mahu Sag stratigraphy can be subdivided into the lower Baikouquan, middle Karamay, and upper Baijiantan Formations that were developed during the Triassic (Fig. 2). The Baikouquan Formation of the

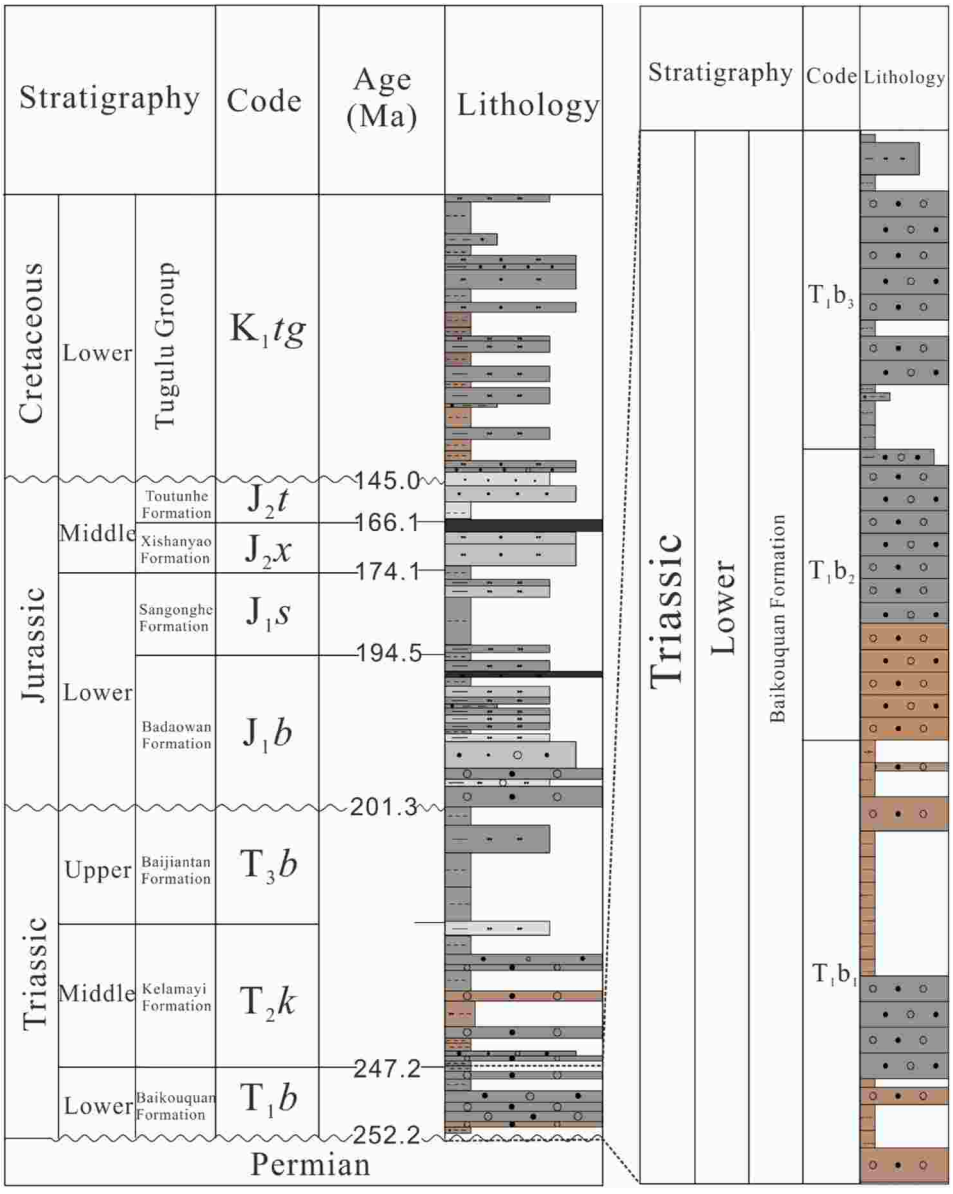

Fig. 2. Synthetical stratigraphic histogram of the strata in the research region. A high-resolution sequence of the target layer is shown on the right (modified from Xinjiang Oilfield).

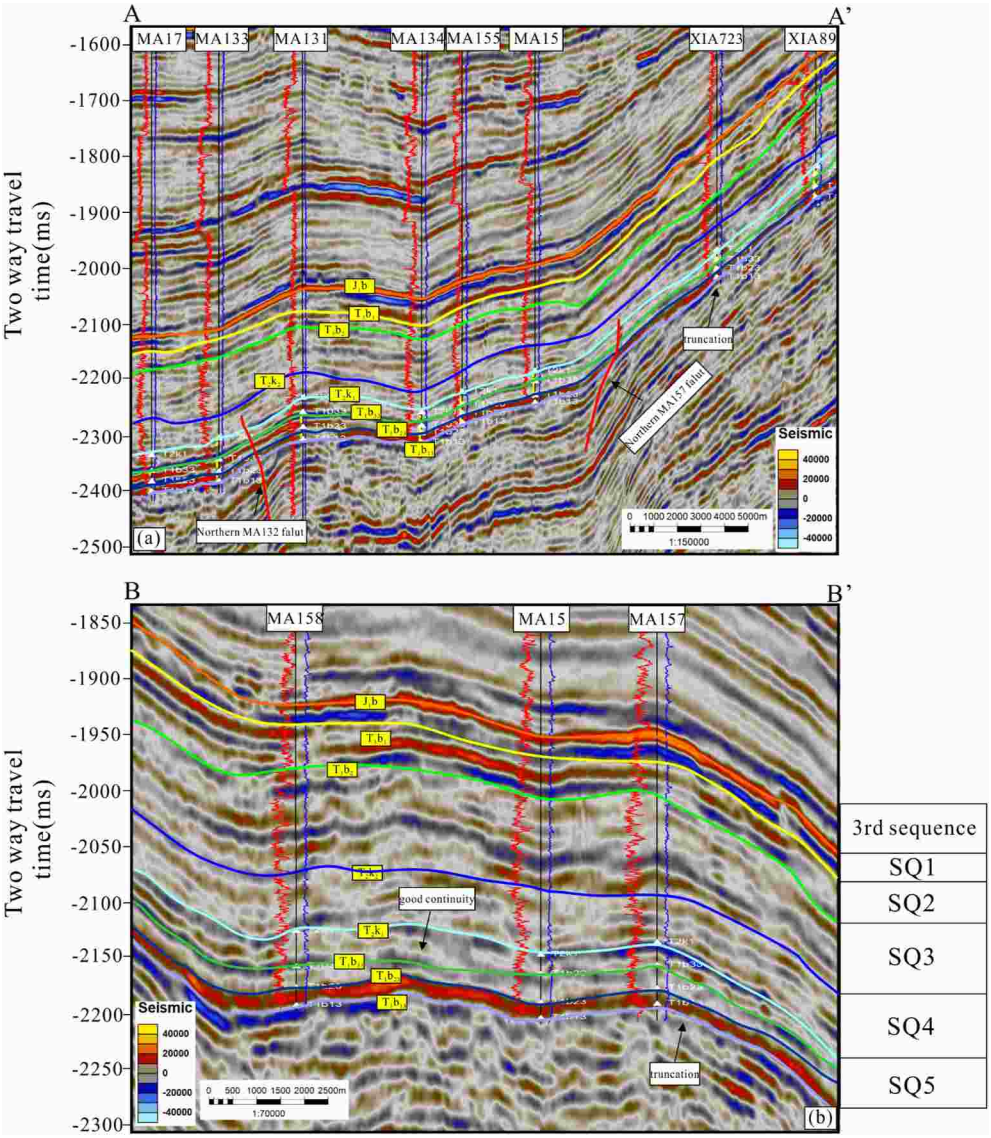

Fig. 3. Interpreted sequence-interface calibration characteristics and the Triassic sequence comparison framework. Fig. 3a depicts the longitudinal section direction and 3b depicts the cross section direction. See Fig. 1c for the location. The column to the right shows the interpreted Triassic sequences SQ1–SQ5. The red well log curve refers to GR, and the blue well log curve refers to RD. (For interpretation of the references to color in this figure legend, the reader is referred to the Web version of this article.)

Lower Triassic is our target stratum, which lies with an angular unconformity upon the underlying lower Wuerhe Formation (P_2w) of the Middle Permian and a conformable contact with the overlying Karamay Formation (T_2k) of the Middle Triassic. Fluviolacustrine deposits of conglomerates that are interbedded with pebbly sandstone, sandstone, and mudstone characterize the Baikouquan Formation (Feng et al., 2019; Xu et al., 2019). The Baikouquan Formation can be further subdivided into three members (Mbr1, Mbr2, and Mbr3). From bottom to top, the retrograded fan deltaic depositional system developed during the lake transgression. Many sets of thick glutenite developed vertically, which facilitated the formation of large-scale high-quality reservoirs and lays the foundation for taking shape lithologic reservoirs.

3. Materials and methodology

3.1. Materials

We used core samples, wireline log data, fluorescence thin sections, casting thin sections, 3D seismic data, and data associated with oil and gas production, which had been obtained for hydrocarbon exploration within the northern Mahu Sag in the Junggar Basin and provided by the Exploration and Development Research Institute of Xinjiang Oilfield Company (CNPC).

The 3D seismic volume covered the entire research region, with 20–50 Hz effective bandwidth, 2 ms vertical sample interval, and 12.5 m × 12.5 m horizontal bin size. The vertical resolution of the seismic data was assumed to be ~23 m on account of a dominant frequency of 30 Hz in the target zone. Thus far, 38 wells have been drilled into the Triassic strata, including 34 vertical and four horizontal wells, with most well depths exceeding 3000 m. Core samples (including thin sections) provide the most direct evidence of lithology and sedimentary microfacies identification. The conventional logs sensitive to lithology included gamma-ray (GR) and formation resistivity (RD), which were used for detailed analysis of the stratigraphy, lithofacies, and sediments. Oil and gas production data from numerous appraisal wells along with some fluorescence thin sections were used in the hydrocarbon accumulation analysis of the study area. Leica polarized light fluorescence microscopy was performed to observe fluid inclusion petrography. Furthermore, the homogeneous inclusion temperature of 32 samples from four wells was measured.

3.2. Methodology

A fifth-order sequence was first constructed by sequence boundary

identification through the pattern of logging curves with high vertical resolution under a fourth-order sequence framework constraint. Subsequently, the sedimentary microfacies were identified based on the core-calibrated logging facies under a fifth-order isochronous stratigraphic framework constrain. Then, extraction of the acoustic impedance (AI) amplitude seismic attribute was performed to ascertain the vertical and planar distributions of the depositional systems and to explain the dynamic sedimentary evolution processes by creating stratigraphic slices in 2 ms intervals. The workflow can be described as follows.

(1) The construction of a high-resolution fifth-order stratigraphic sequence framework of the Baikouquan Formation was performed.
(2) The sedimentary microfacies were accordingly determined via interpretation of the core-calibrated logging facies. Extraction of the AI amplitude seismic attribute was done to ascertain the vertical and planar distributions of the depositional systems.
(3) The examination of the filling and evolution processes of the sedimentary system under the fifth-order sequence framework was carried out by applying stratigraphic slices in 2 ms intervals.
(4) The hydrocarbon accumulation analysis of the study area used fluorescence thin sections, measured homogeneous inclusion temperature, and oil as well as gas production data.
(5) Afterward, the main hydrocarbon reservoir models were summarized according to the conditions and characteristics under which the hydrocarbon reservoirs formed. Eventually, the hydrocarbon enrichment law governing the different types of hydrocarbon reservoirs was discussed.

4. Results

4.1. Sequence stratigraphy

Statistically, 86% of the reserves of most oil and gas fields in the world may be located in the lowstand system tract (LST), 12% in the transgressive system tract, and 2% in the highstand system tract (Melo et al., 2021; Shang et al., 2022). Accordingly, the enrichment law of hydrocarbon accumulation is highly correlated with the types of system tract in the sequence stratigraphy. The substantial majority of hydrocarbon reservoirs distributed in the LST of sequences are subtle reservoirs, such as stratigraphic and lithologic reservoirs, including lithologic lens formed in the basin floor and underwater fans, stratigraphic pinch-out reservoirs associated with the delta or estuary formed near the progradational wedge, and oil and gas reservoirs associated with ancient river channels traced upward against the estuary (Bahmani et al., 2020). Thus, investigating the sequence stratigraphy is an essential and effective strategy for providing a foundation to locate stratigraphic lithologic reservoirs.

4.1.1. Sequence boundaries

The Junggar Basin is in a foreland basin phase and the study interval Baikouquan Formation is dominated by proximal fan delta deposits, developing several sets of thick sandy conglomerates (Wu et al., 2020). Hence, the classic sequence stratigraphy mainly employed in the marine facies stratum near the passive continental margin is no longer applicable for the fine sequence division of the strata in the study area (Vail, 1987). Furthermore, deep burial depth, thin thickness strata characterize the Baikouquan Formation (~1 km); hence, accurately identifying the stratigraphic sequence boundary is difficult. A high-resolution sequence stratigraphy is highly recommended, integrating results obtained from seismic data, well logs, and core samples to reconstruct the sequence framework for subsequent sedimentary analysis and subtle reservoir identification.

A high-resolution sequence stratigraphic framework of the Baikouquan Formation was reconstructed according to the 3D seismic data and appraisal wells in the research region via a fine-synthetic seismogram. The Triassic in the northern Mahu Sag was further subdivided into five third-order sequences, where the internal seismic events had good continuity (Fig. 3). The Baikouquan Formation is a third-order sequence at the bottom of the Triassic. The top interface of the Baikouquan Formation represents a lacustrine flood surface, which is the conversion interface between a set of fine-grained deposits in the late stage of the Baikouquan Formation and grayish-green sandy conglomerates of the lower Karamay Formation (Fig. 4). The seismic reflector marks a conformable contact (Fig. 3), and the log curve abruptly changes from low resistivity to high resistivity (Fig. 4). The bottom interface of the Baikouquan Formation denotes an angular unconformity between the underlying Permian and the overlying Triassic. It could be recognized with truncation and onlap characteristics observed on the seismic profile (Fig. 3). Because of the resolution of the seismic data, the fifth-order sequence boundaries can only be determined via geophysical logging responses and core samples. The target interval in the study area is predominantly terrigenous coarse clastic deposits containing high shale content, which indicated that the natural GR curve cannot precisely reflect the cycle characteristics. The fifth-order sequence boundaries in accordance with the changes in particle size and sedimentary energy are mainly inferred, synthesizing the natural GR and RD curves. Therefore, the Baikouquan Formation was divided into nine fifth-order sequences (SSQ1–SSQ9) in the wells (Fig. 4).

4.1.2. Sequence stratigraphic analysis

The fourth-order sequence Mbr 1 of the Baikouquan Formation comprises SSQ1–SSQ3. SSQ1 and SSQ2 correspond to the lower Mbr 1, with the lithology mainly comprising grayish brown sandy conglomerates interbedded with thin mudstones (Fig. 4a). The GR log curves of SSQ1 and SSQ2 were mainly bell-shaped and funnel-shaped, respectively (Fig. 4a), with the characteristics of thinning upward and coarsening, indicating the lake transgression in SSQ1 and regression in SSQ2. SSQ3 corresponds to the upper part of Mbr 1, with the lithology predominantly comprising dark-gray massive sandy conglomerates. Medium-to-low GR values and high RD values are observed for the conventional logging response. A thick box shape can be seen in the RD curve (Fig. 4a), with obvious serrated features, corresponding to an oscillatory transgressive sedimentary process.

SSQ4–SSQ6 constitute Mbr 2 of the Baikouquan Formation, where SSQ4 and SSQ5 correspond to the lower part and SSQ6 corresponds to the upper part. The lithology of the lower part of Mbr 2 is mainly green–gray matrix–supported conglomerate characterized by poorly sorted and substantial high muddy content (Fig. 4a). The gravel clasts are suspended in the muddy matrix. Generally, they are characterized by stacked massive beddings. Such rock facies are formed via debris-flow deposition. A high GR value and low RD value are observed for the conventional well log. The lithology of the upper part of Mbr 2 comprises gray sandy conglomerate interbedded with brown mudstone. A low GR value and high RD value can be observed in the logging curve, and there are no obvious serrated features (Fig. 4b), indicating a sufficient accommodation space and relatively stable deposition process.

Mbr 3 of the Baikouquan Formation comprises SSQ7–SSQ9. SSQ7 corresponds to the lower Mbr 3, with the lithology mainly comprising reddish-brown mudstones interbedded with thin sandstones. High GR and low RD values can be observed in the log curve (Fig. 4a). SSQ8 corresponds to the middle part of Mbr 3. Its lithology comprises gray conglomerate with thin sandstones and exhibits the characteristic of coarsening upward. A serrated box shape can be seen in the RD curve (Fig. 4b). SSQ9 corresponds to upper Mbr 3, with a lithology and logging response similar to those of SSQ7.

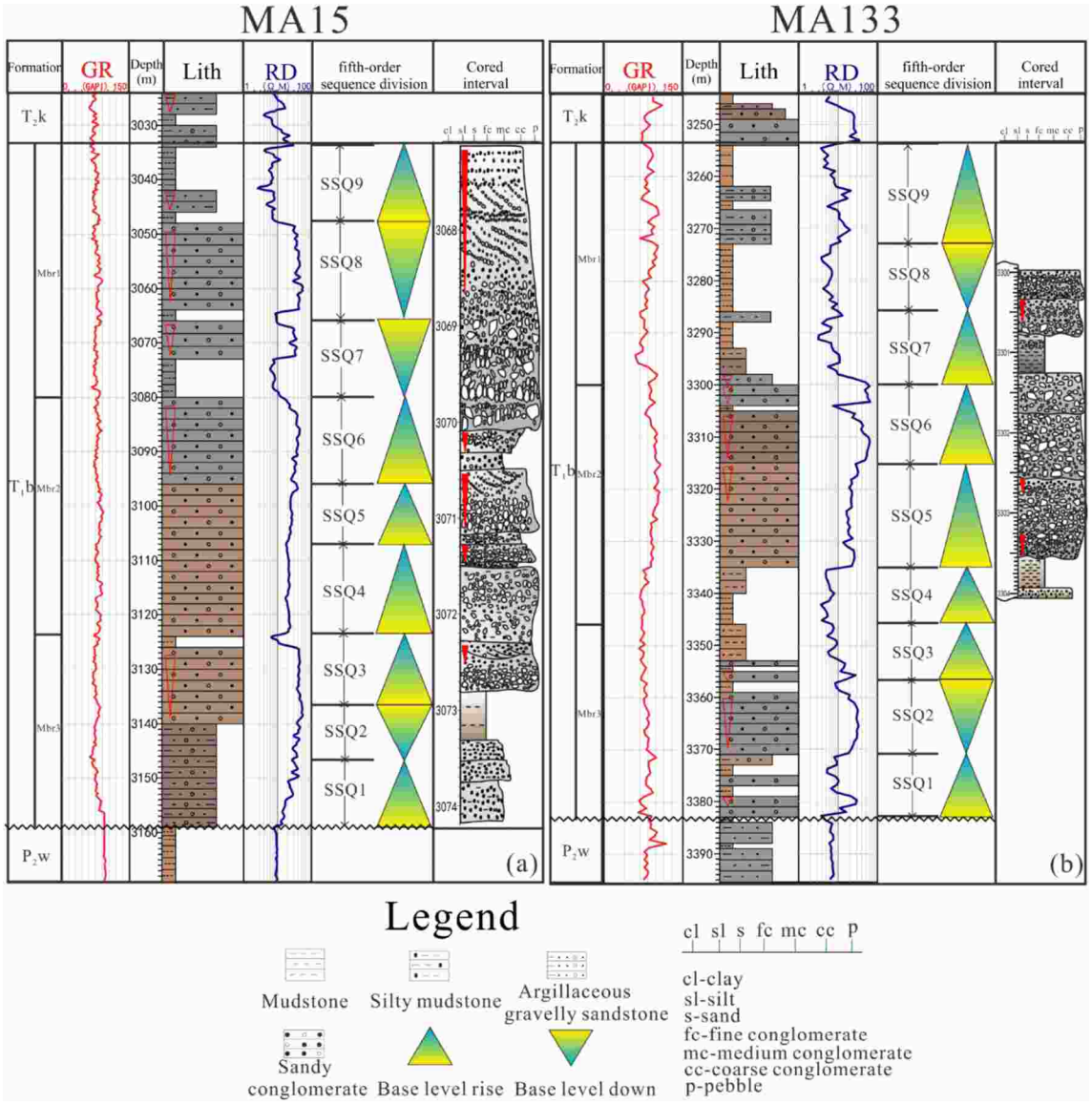

Fig. 4. Division of the fifth-order sequence of the Baikouquan Formation in the MA133 and MA15 wells. See Fig. 1c for the locations of the wells.

4.2. Sedimentary facies

4.2.1. Sedimentary facies type

4.2.1.1. Fan-delta plain. The fan delta plain has characteristics very similar to those of the root fan and inner-middle fan of the alluvial fan, both of which are coarse-grained sedimentary bodies formed under an aquatic oxidation environment. The sedimentary deposits are generally brown, brownish-red conglomerate, and sandy conglomerate packed with sandstones as well as mudstones. Debris flow, braided river channel, and overflow can be observed in the fan-delta plain, which is dominated by the former two microfacies.

(1) Debris flow

Debris flow deposition forms the principal part of the fan delta plain. It was a coarse-grained, sheet-shaped hybrid accumulation spreading at the mountain pass, carrying a large amount of mud, sand, and gravel sediments within the flood during the disaster period. The lithology comprised brown and brownish-red thick medium-grained conglomerate or pebbly sandstone. The typical sedimentary characteristic was marked by a matrix-supported structure, medium-to-poor sorting (Fig. 5), and subangular-to-angular particles. The gravel sizes were generally in the range of 0.6–40 mm, with a maximum particle size up to 100 mm. The gravel particles were suspended in the sandy or muddy matrix locally and exhibited disorderly arrangement, without any directionality and imbrication.

(2) Braided river channel

The lithology comprised brown, brownish-red, medium-to-fine grained conglomerate, pebbly sandstone, and sandstone, dominated by conglomerate (82%). The sorting was medium to poor, and the roundness characteristics suggested that the gravels were mainly subangular and subrounded. The gravels at the bottom of the river channel generally exhibited an imbricate orientation and low-angle crossbedding (Fig. 5) in the middle and lower parts of the channel. A relatively low content of the argillaceous matrix was found (generally <5%). From the bottom to the top, the complete channel exhibited the normal-graded sequence transited from imbricated pebble to crossbedding conglomerate, pebbly sandstone, and to parallel bedding or massive bedding sandstone.

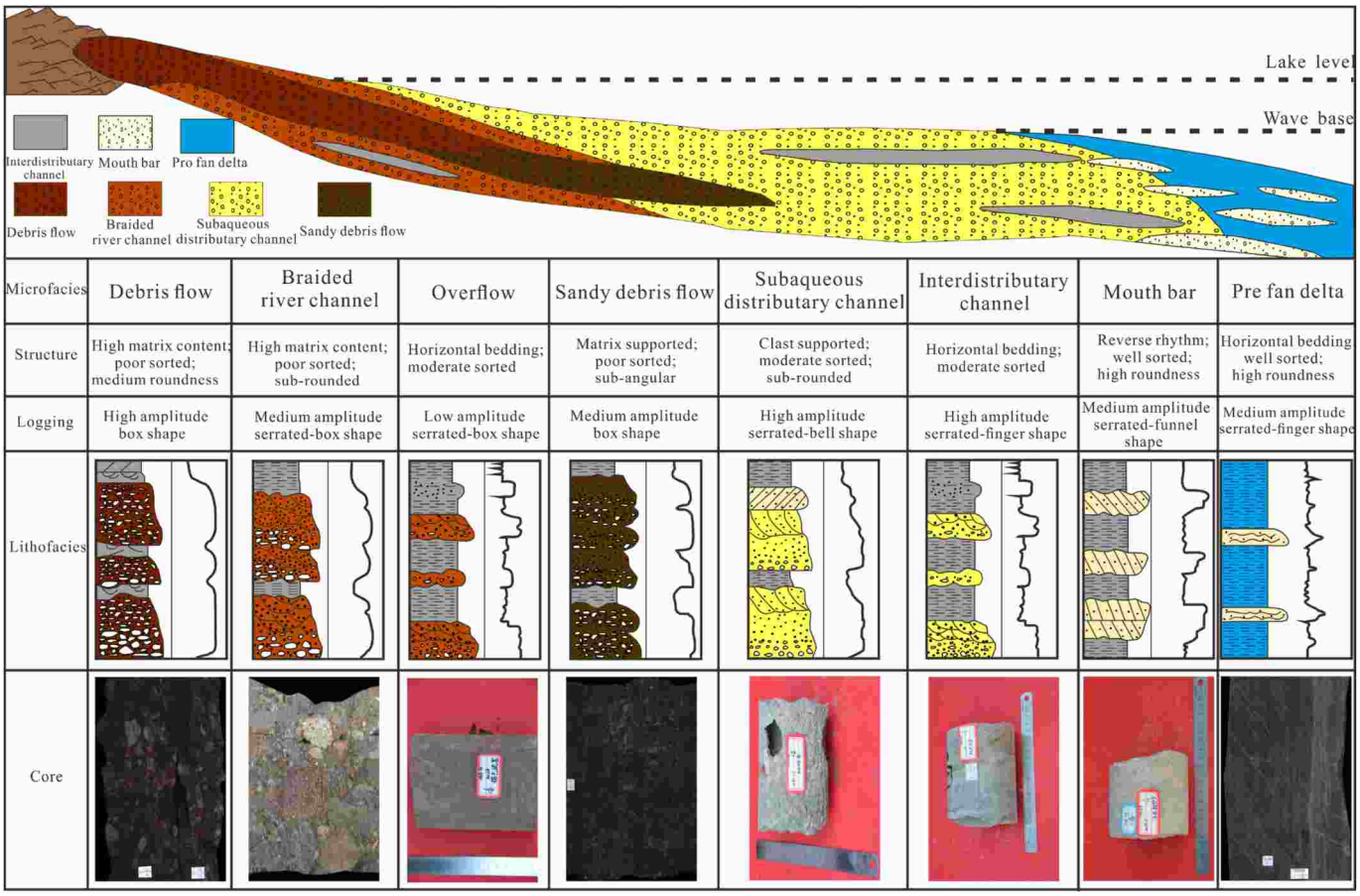

Fig. 5. Logging responses, core photos, and structure characteristics of different microfacies in the fan-delta complex.

(3) Overflow

The overflow sediments comprised brown and brownish-red, medium-thin mudstone and siltstone, of which plant fossils may be recorded (Fig. 5). Because of the incision and erosion of debris flow and braided river channel, the single layer produced was mostly <0.3 m and developed mass bedding.

4.2.1.2. Fan-delta front. The underwater part of the fan delta comprises the fan-delta front and prefan delta, which is the most important evidence differentiating it from alluvial-fan deposits. The fan-delta front sediments were generally grayish-green conglomerates and sandy conglomerates packed with sandstones and mudstones. Detailed core observations revealed that there are four types of microfacies: sandy debris flow (underwater debris flow), subaqueous distributary channels, interdistributary channels, and mouth bars, with sandy debris flow and subaqueous distributary channels being dominant (90%).

(1) Sandy debris flow

Sandy debris flow is the underwater extension of debris flow in the plain environment. It had similar sedimentary characteristics with debris flow and the lithology comprised grayish-green, medium-grained conglomerate and sandy conglomerate. The gravel exhibited poor sorting, low roundness, and subangular characteristics, without directionality and imbrication (Fig. 5). Huge gravels were suspended in the sandy matrix, without bedding and other sedimentary structures.

(2) Subaqueous distributary channels

The lithology comprised grayish-green, fine-grained conglomerate, pebbly sandstone, and sandstone. They were poorly-to-moderately sorted and their psephicity is commonly subrounded-to-subangular shapes, representing tractive current deposits that evolved mainly in underwater distributary channels. Oil spots were identified (Fig. 5). Matrix-supported conglomerates have higher density, while higher resistivity and lower density values were found for the clast-supported conglomerates. There were observed low-angle cross-bedding and parallel bedding in the middle lower part of the channel. The normal-graded sequence commonly occurred from the fine-grained conglomerate to pebbly sandstones as well as sandstones from bottom to top in the channel. The deposits of subaqueous distributary channels could extend further than those in the sandy debris flow, which usually deposited at the proximal fan-delta front.

(3) Mouth bars and interdistributary channels

Because of the erosion of debris flow, preservation of mouth bars was hard and it results in their low development. The lithology comprised medium sandstone, coarse sandstone, and pebbly sandstone, forming a reverse-graded sequence (Fig. 5). Interdistributary channels were characterized by fine-grained sediment deposited between subaqueous distributary channels, which mainly comprised grayish-green mudstones and siltstones.

4.2.1.3. Prefan delta. Dark-gray and dark horizontal bedding mudstones primarily comprise the prefan delta, with some locally developed thin sandy debris flow deposits (Fig. 5).

4.2.2. Sedimentary evolution

The provenances were afforded by the northern Xiazijie fan and the eastern Madong fan based on the studies investigating the ZTR index of stable heavy minerals. By integrating the results obtained via the ZTR index with those from dominant microfacies of the single well, sand (sandstone and conglomerate) strata ratio, and extraction of seismic inversion cube, the final sedimentary microfacies of the Baikouquan Formation were interpreted to follow the fifth-order sequence boundaries. Stratal slices were employed to produce seismic facies maps within an isochronous sequence stratigraphic framework, which could more precisely delineate the lithologic features and sedimentary environment. Herein, the top and bottom interfaces of the seismic events of the Baikouquan Formation were selected as the reference layers for their globally continuous and traceable characteristics. Fig. 6 (panels a–f) depicts the six evolutionary stages of the fan delta systems during the deposition of the Baikouquan Formation. The northern Xiazijie fan delta system and the eastern Madong fan delta system are identified using stratal slices.

SSQ1–SSQ3 (Fig. 6a): in the early stage of the Baikouquan Formation, there was a considerably lower accommodation-space expansion rate than the supplying rate of the sediment. The Xiazijie fan in the north and the Madong fan in the east accumulated, characterized by rapid progradation. During this period, the subaqueous distributary channel of the fan-delta front exhibited a wide distribution to the south of wells MA153 and MA158, whereas the sandy debris flow was distributed to the south of well MA131. The SSQ1 sequence was marked by a large area of fan-delta front and sandy debris flow in the research region. A few mouth bars were developed in the southern portion near well MA137.

SSQ4 (Fig. 6b): at this stage, both the Xiazijie fan and the Madong fan prograded because of a fall in the lacustrine level. The sediment supply of the Xiazijie fan was sufficient and the fan-delta plain subfacies belt was found to migrate from well XIA723 to the south of well XIA722. The fan-delta front subfacies had retreated to the north of well MA154 because of the progradation of the sandy debris flow afforded by the Madong fan in the east. The isolated mouth bars were developed near wells MA137 and MA133. Generally, relatively developed sand bodies in this sequence were observed, with coarse particle size.

SSQ5 (Fig. 6c): dominant extensive sandy debris flow was found in the southern portion of the research region, of which the microfacies belt gradually migrated to the south of well MA133. Conversely, the fan-delta plain of the Xiazijie fan had retrograded to the south of well XIA723. The sand bodies of the fan-delta front exhibited the characteristics of good connectivity and were developed to the north of well MA154. Simultaneously, the mouth bars were not developed and the lacustrine deposits were only distributed within a narrow area in the southern portion of the research region.

SSQ6 (Fig. 6d): during the middle stage of the Baikouquan Formation, a gentle paleotopography had formed following the earlier sedimentary filling process. Hence, the sandy debris flow was not developed because of the control of the offloading of gravity flow sand bodies by an abrupt paleotopographic slope break. In addition, because of the rise in the lake level, the fan-delta plain had disappeared because of the retrogradation of the Xiazijie fan in the north. Therefore, this sequence was dominated by the fan-delta front over a large area in the study area. The isolated mouth bars were distributed near well MA17.

SSQ7–SSQ8 (Fig. 6e): at this stage, the Xiazijie fan continuously retrograded and the microfacies belt of the fan-delta front migrated to the north of well MA132. The sand bodies of the fan-delta front exhibited relatively stable thickness and continuous development. In addition, the scale of the mouth bars in the fan-delta front had increased and the interdistributary channels were developed locally near well MA156.

SSQ9 (Fig. 6f): during the late stage of the Baikouquan Formation, there was decreased sediment supply of the Xiazijie fan, possibly caused by a sharp increase in the lake level. In this period, the sequence was dominated by muddy deposits of interdistributary channels and sand bodies of the subaqueous distributary channels. The sand bodies of the subaqueous distributary channels were broom-shaped and developed centered around wells MA155 and XIA723.

4.3. Genetic type of hydrocarbon models

Table 1 shows the formation pressure and physical properties of crude oil in each fault block of the Baikouquan Formation. The formation pressure factors of MA133, MA131, and XIA72 fault blocks were 1.23, 1.27, and 0.88, respectively. Furthermore, properties of crude oil and saturation degree have distinct characteristics. These results indicate that the fault block has a substantial control on the reservoir hydrocarbon accumulation. The primary source rocks of the Mahu Sag are the Permian Fengcheng (P_1f) and Wuerhe (P_2w) Formations. A recent study proposed that mainly two hydrocarbon charging periods exist in the Baikouquan Formation (Pan et al., 2021). In summary, the first phase of hydrocarbon charging occurred during the Early Jurassic, trapping yellow-fluorescent inclusions which appear mainly in intergranular pores, fractures, and quartz (Fig. 7a, b, c). The second phase of hydrocarbon charging occurred during the Early–Middle Cretaceous, trapping blue-fluorescent hydrocarbon inclusions mainly occurring in feldspar-dissolution pores and fractures (Fig. 7c, d, e, f). Moreover, the two homogenization temperature intervals associated with the two oil charging times correspond to the Early Jurassic and Early–Middle Cretaceous. The results indicate a homogenization temperature range of 70 °C–90 °C of aqueous inclusions associated with yellow-fluorescent hydrocarbon inclusions and a homogenization temperature range of 100 °C–120 °C of aqueous inclusions associated with blue-fluorescent hydrocarbon inclusions (Fig. 8).

As for the MA131 well block, a single peak distribution is observed for the homogenization temperature of aqueous inclusions in the XIA72 and MA133 fault block reservoirs, indicating only one period of hydrocarbon charging while two periods of hydrocarbon charging are found for the MA131 fault block from the Fengcheng and Wuerhe Formations. Among the three fault blocks, the hydrocarbon in the XIA72 fault block mainly comes from the source rock belonging to the Fengcheng Formation connected with deep faults. During the Early Jurassic, the source rock belonging to the Fengcheng Formation matured and hydrocarbon migration occurred to accumulate and migrate into structural highs in the XIA72 fault block, realizing an adequate hydrocarbon charging, yielding a “grain with oil inclusion” (GOI) of ~10% (Fig. 8). The MA131 fault block reservoir had undergone this stage of hydrocarbon charging, with a GOI of ~8%. Afterward, with the further burial of the entire depression, the source rock of the Wuerhe Formation matured and generated hydrocarbons in the later stage. The deep fault dividing the MA131 and XIA72 fault blocks had been closed. Hence, the MA131 fault block is the primary crude oil mixing area, whereas the lower MA133 fault block has relatively few mixed sources because of the adequate hydrocarbon charging of the Wuerhe Formation in the later stage.

Based on source rocks, faults, and reservoirs, there are nine categories of the hydrocarbon reservoir models of the study area given as follows (Fig. 9): the lithologic hydrocarbon reservoir model with braided river sand bodies and oil from the Fengcheng Formation (Fig. 9a), lithologic hydrocarbon reservoir model with distributary channel sand bodies and oil from the Fengcheng Formation (Fig. 9b), fault-lithologic hydrocarbon reservoir model with distributary channel sand bodies and oil from the Fengcheng Formation (Fig. 9c), lithologic hydrocarbon reservoir model with distributary channel sand bodies and mixed oil (Fig. 9d), laterally screened hydrocarbon reservoir model with distributary channel sand bodies and mixed oil (Fig. 9e), fault-lithologic hydrocarbon reservoir model with distributary channel sand bodies and mixed oil (Fig. 9f), fault-lithologic hydrocarbon reservoir model with distributary channel sand bodies and oil from the Wuerhe Formation (Fig. 9g), lithologic hydrocarbon reservoir model with distributary channel sand bodies and oil from the Wuerhe Formation (Fig. 9h), and

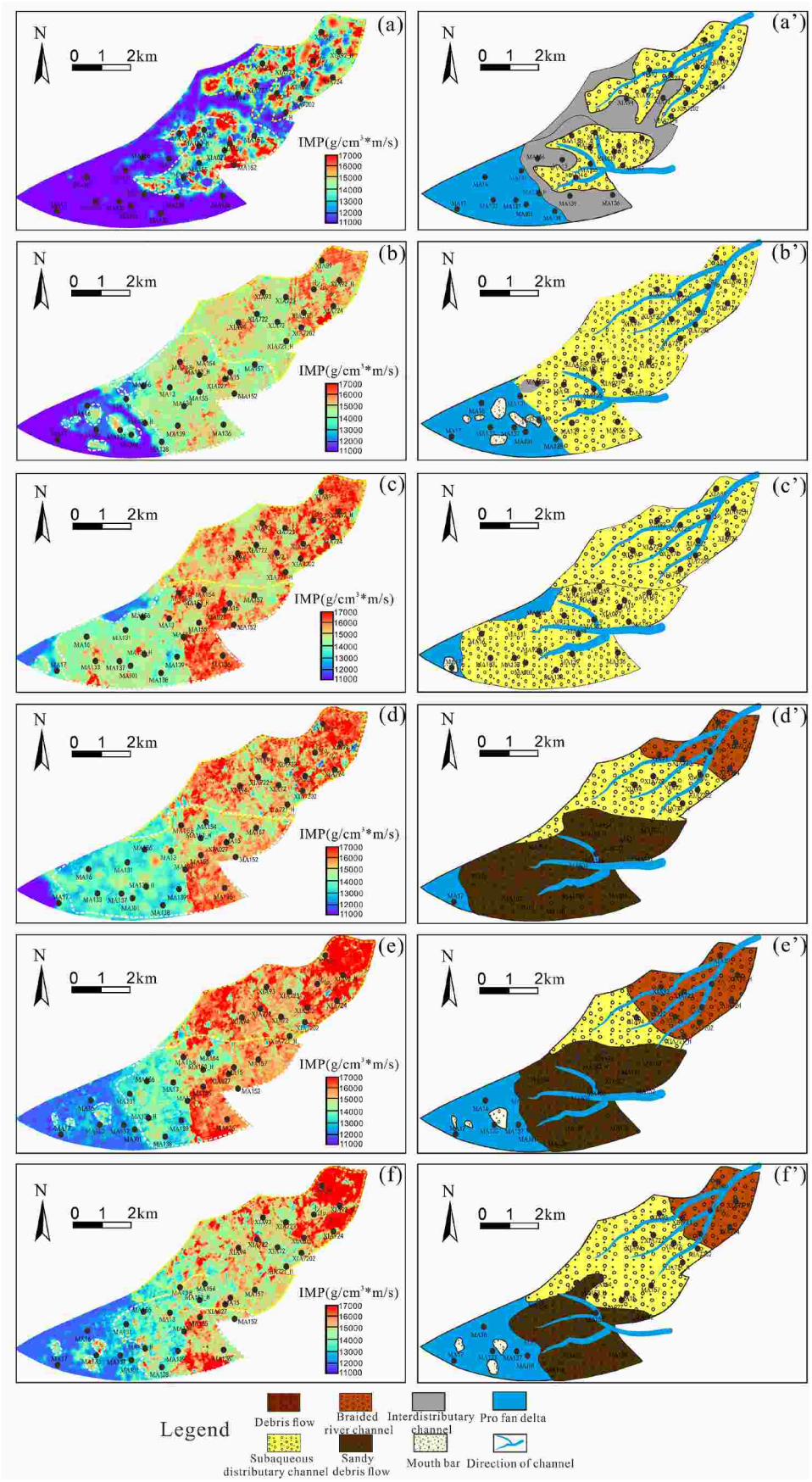

Fig. 6. Acoustic impedance stratigraphic slices and sedimentary-facies interpretations of the representative stratigraphic attributes of different fifth-order sequences. (a) SSQ1–SSQ3 corresponds to the first member of the Baikouquan Formation. (b) SSQ4 corresponds to the lower portion of the second member of the Baikouquan Formation. (c) SSQ5 corresponds to the middle portion of the second member of the Baikouquan Formation. (d) SSQ6 corresponds to the upper portion of the second member of the Baikouquan Formation. (e) SSQ7–SSQ8 corresponds to the lower portion of the third member of the Baikouquan Formation. (f) SSQ9 corresponds to the upper portion of the third member of the Baikouquan Formation.

Table 1
Formation pressure and physical properties of crude oil in each fault block in the Baikouquan Formation.

Fault block	Density (g/cm^3)	Viscosity (mPa.s)	Wax content (%)	Formation pressure (MPa)	Formation pressure coefficient	Saturation degree (%)	Reservoir temperature (°C)	Freezing point temperature (°C)	Initial boiling point (°C)
MA133	0.8009	1.52	4.34	40.33	1.23	87.99	79.61	−6.00	91.00
MA131	0.8207	5.82	4.97	38.78	1.27	87.51	74.87	−1.76	121.67
XIA72	0.8404	7.58	4.92	23.95	0.88	80.41	68.07	4.40	135.30

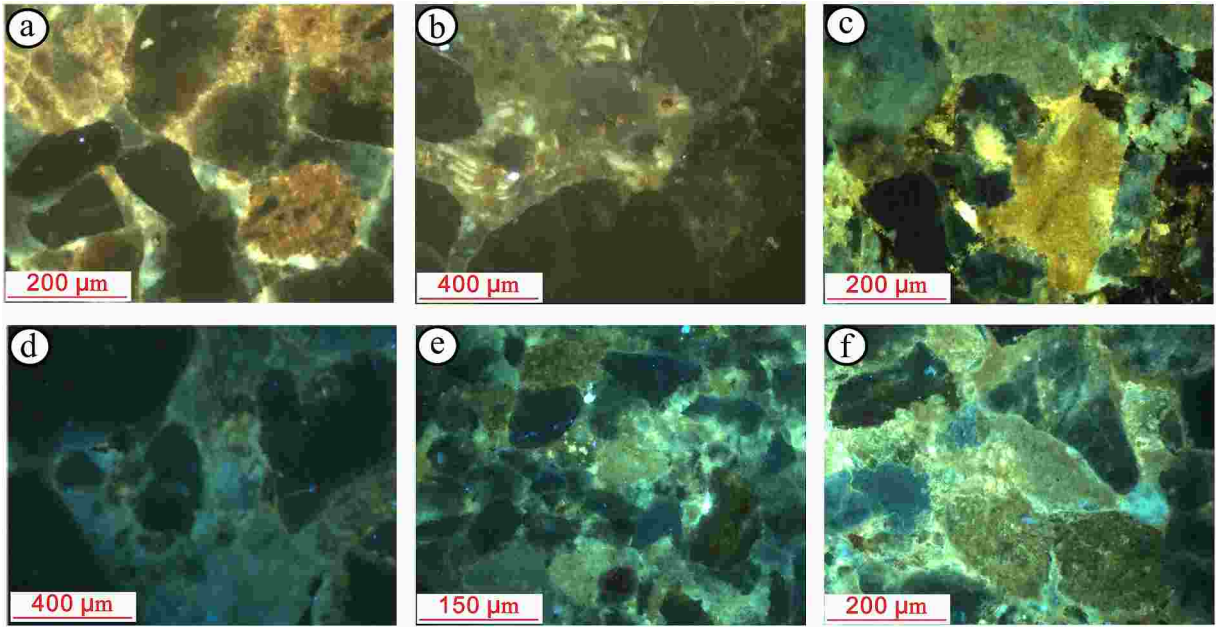

Fig. 7. Fluorescence photomicrographs showing the range in colors exhibited by the oil inclusions. (a) hydrocarbon with yellow fluorescence preserved in quartz and matrix, well XIA92, 2506.90 m. (b) liquid hydrocarbons with yellow fluorescence observed in quartz particle, well XIA89, 2447.00 m. (c) yellow-fluorescent hydrocarbon preserved in the detrital grain and blue-fluorescent hydrocarbon filling the matrix, representing two phases hydrocarbon charging, well MA15, 3069.78 m. (d) little yellow-fluorescent hydrocarbon exhibited in the matrix and blue-fluorescent hydrocarbon preserved in the matrix and detrital grain, representing two phases hydrocarbon charging, well MA134, 3193.33 m. (e) hydrocarbon with blue fluorescence preserved in detrital grains and matrix, well MA17, 3249.33 m. (f) liquid hydrocarbons with blue fluorescence filling the dissolved feldspar pores and matrix, well MA16, 3213.84 m. (For interpretation of the references to color in this figure legend, the reader is referred to the Web version of this article.)

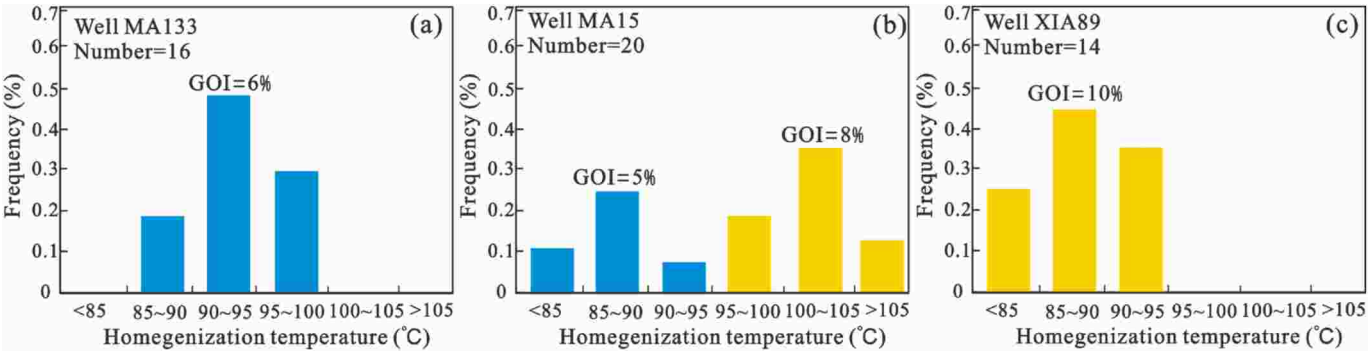

Fig. 8. Measured homogenization temperatures of the aqueous inclusions. (a), (b), and (c) represents the samples obtained from MA133, MA131, and XIA72 fault blocks, respectively. The yellow column indicates that the inclusions are mainly developed in the early stage of quartz overgrowth, and the blue column represents the inclusions developed during or after the late stage of quartz overgrowth. (For interpretation of the references to color in this figure legend, the reader is referred to the Web version of this article.)

lenticular lithologic hydrocarbon reservoir model with mouthbar sand bodies and oil from the Wuerhe Formation (Fig. 9i). Lithologic hydrocarbon reservoirs are the most typical and important hydrocarbon reservoir models discovered in the study area, which are identified in many wells and mainly developed vertically in SSQ6–SSQ8 (Table 2). The reservoir sand bodies primarily comprise a distributary channel and braided river, of which the updip direction is gradually lithologically pinched out. The fault-lithologic hydrocarbon reservoirs are distributed around the corresponding main control fault, which blocks the updip reservoir sand body, such as those seen in wells XIA72, MA133, and MA131 (Table 2, Fig. 10). The lenticular lithologic hydrocarbon reservoirs are mainly developed in a shallow lake in the MA133 fault block,

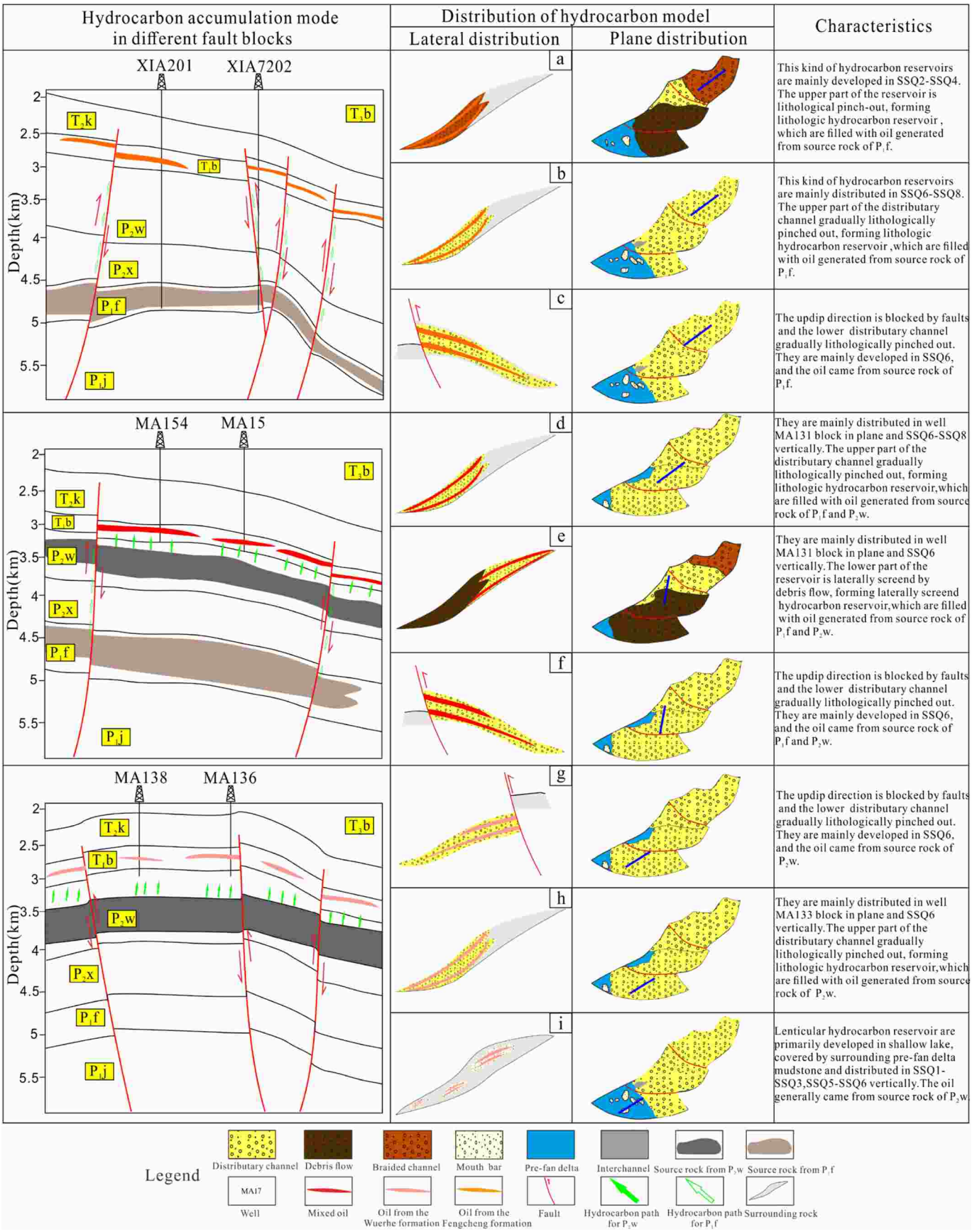

Fig. 9. Hydrocarbon accumulation mode and types of hydrocarbon reservoir models in the MA131 well block.

Table 2
The characteristics of different hydrocarbon reservoirs in different fault blocks.

Fault block	Well name	Fifth-order sequence	Type of hydrocarbon reservoirs	Microfacies	Source oil	Distance from the main control fault (m)	Effective reservoir thickness (m)	Cumulated oil (t)
XIA72	XIA72	SSQ6	fault-lithologic hydrocarbon reservoir	distributary channel	P_1f	2045	6.8	131.48
	XIA89	SSQ6	lithologic hydrocarbon reservoir	distributary channel	P_1f	1078	8.3	162.45
	XIA89	SSQ4	lithologic hydrocarbon reservoir	braided river	P_1f	1186	7.9	/
	XIA93	SSQ6	lithologic hydrocarbon reservoir	distributary channel	P_1f	1756	5.4	81.89
	XIA93	SSQ4	lithologic hydrocarbon reservoir	braided river	P_1f	1538	6.9	/
	XIA94	SSQ6	fault-lithologic hydrocarbon reservoir	distributary channel	P_1f	1953	5.2	92.29
	XIA94	SSQ8	fault-lithologic hydrocarbon reservoir	distributary channel	P_1f	2028	4.8	/
	XIA7202	SSQ6	lithologic hydrocarbon reservoir	distributary channel	P_1f	987	9.5	141.45
	XIA7202	SSQ7	lithologic hydrocarbon reservoir	distributary channel	P_1f	863	11.7	358.05
	XIA723	SSQ6	lithologic hydrocarbon reservoir	distributary channel	P_1f	3365	4.1	63.91
	XIA723	SSQ2	lithologic hydrocarbon reservoir	braided river	P_1f	2789	5.6	/
	XIA724	SSQ7	lithologic hydrocarbon reservoir	distributary channel	P_1f	1213	8.3	117.75
MA133	MA133	SSQ6	lithologic hydrocarbon reservoir	distributary channel	P_2w	2048	13.6	1091.51
	MA133	SSQ2	lenticular lithologic hydrocarbon reservoir	mouth bar	P_2w	2232	8.7	/
	MA136	SSQ6	lithologic hydrocarbon reservoir	distributary channel	P_2w	1876	5.4	/
	MA136	SSQ7	lithologic hydrocarbon reservoir	distributary channel	P_2w	1965	4.7	71.3
	MA137	SSQ6	lithologic hydrocarbon reservoir	distributary channel	P_2w	2566	6.5	123.95
	MA138	SSQ6	lithologic hydrocarbon reservoir	distributary channel	P_2w	1876	4.1	62.77
	MA139	SSQ6	lithologic hydrocarbon reservoir	distributary channel	P_2w	1759	3.5	29.18
	MA139	SSQ7	lithologic hydrocarbon reservoir	distributary channel	P_2w	1654	8.3	258.57
	MA16	SSQ6	fault-lithologic hydrocarbon reservoir	distributary channel	P_2w	1341	11.2	965.41
MA131	MA13	SSQ6	lithologic hydrocarbon reservoir	distributary channel	mixed	2542	6.5	/
	MA13	SSQ7	lithologic hydrocarbon reservoir	distributary channel	mixed	2359	6.9	114.71
	MA131	SSQ6	fault-lithologic hydrocarbon reservoir	distributary channel	mixed	1315	11.6	1601.3
	MA134	SSQ6	laterally screened hydrocarbon reservoir	distributary channel	mixed	663	2.5	7.44
MA131	MA134	SSQ7	lithologic hydrocarbon reservoir	distributary channel	mixed	576	13.8	1464.6
	MA15	SSQ7	fault-lithologic hydrocarbon reservoir	distributary channel	mixed	3534	10.8	405.1
	MA15	SSQ6	fault-lithologic hydrocarbon reservoir	distributary channel	mixed	3238	4.2	55.71
	MA152	SSQ8	fault-lithologic hydrocarbon reservoir	distributary channel	mixed	112	6.6	148.38
	MA154	SSQ7	lithologic hydrocarbon reservoir	distributary channel	mixed	3646	2.5	27.84
	MA154	SSQ6	lithologic hydrocarbon reservoir	distributary channel	mixed	3468	3.9	73.03
	MA155	SSQ5	laterally screened hydrocarbon reservoir	distributary channel	mixed	1876	5.4	/
	MA155	SSQ6	lithologic hydrocarbon reservoir	distributary channel	mixed	1783	7.6	155.53
	MA155	SSQ7	lithologic hydrocarbon reservoir	distributary channel	mixed	1654	2.1	11.66
	MA156	SSQ6	laterally screened hydrocarbon reservoir	distributary channel	mixed	1546	4.6	17.93
	MA157	SSQ6	fault-lithologic hydrocarbon reservoir	distributary channel	mixed	984	6.3	54.18

(*continued on next page*)

Table 2 (*continued*)

Fault block	Well name	Fifth-order sequence	Type of hydrocarbon reservoirs	Microfacies	Source oil	Distance from the main control fault (m)	Effective reservoir thickness (m)	Cumulated oil (t)
	MA157	SSQ8	fault-lithologic hydrocarbon reservoir	distributary channel	mixed	1015	3.1	20.16
	MA158	SSQ6	lithologic hydrocarbon reservoir	distributary channel	mixed	2432	1.7	2.51

which are covered by the surrounding prefan-delta mudstone (Table 2, Fig. 10). The oil production and effective reservoir thickness in the XIA72 fault block are highly correlated with the distance between the single well and the main control fault (Table 2). This is because the lower source oil from the Fengcheng Formation migrated upward along the fault to the reservoir developed in the sequence, forming a series of hydrocarbon reservoirs. In the MA133 fault block, lateral and vertical hydrocarbons migrate from the source rocks from the Wuerhe Formation to the reservoir sand bodies through unconformities between the Wuerhe Formation and the Baikouquan Formation. Hence, the oil and gas enrichment of the hydrocarbon reservoirs depends on high-quality reservoirs and the vertical contact relationship between reservoirs and source rocks. Overall, there is relatively better oil and gas enrichment of the hydrocarbon reservoirs in the MA131 fault block than in the other well blocks because two phases of hydrocarbon charging exist with mixed oil and the favorable reservoirs are well developed (Table 2).

5. Discussion

5.1. Depositional model of fan delta deposits

During the deposition of the Baikouquan Formation in the study area, the paleogeomorphology exhibited the characteristics of "nose-shaped highs developed in the middle area of the MA131 well block and deep and steep trenches developed in the east." Under such paleogeomorphic conditions, the local gentle paleogeomorphic slope break distributed in the nose-shaped highs primarily controlled the offloading of traction flow deposits. Conversely, the offloading of gravity flow deposits was influenced by the eastern abrupt slope break. In general, results show that the flow pattern and the distribution range of sand bodies were controlled by the paleogeomorphology. Furthermore, climate was crucial in the sedimentary filling process of the fan delta complex. In an arid–semiarid climate, few plants existed for soil-fixing, causing frequent paroxysmal floods and debris flow after the rainy season, forming a fan delta complex containing much higher gravity flow deposits. Conversely, the long-term stable traction currents occurred under a humid climate. The measured SiO_2-to-Al_2O_3 ratios by the core samples were in the range of 2.8–3.9, indicating that the climate was humid during the deposition of the Baikouquan Formation. Moreover, abundant plant fossils were identified in the rock sample of the Baikouquan Formation, suggesting that the plants were flourishing and there was a humid climate during that time.

Using the aforementioned sedimentary characteristics and evolution process, paleogeomorphology, and paleoclimate, we established a large-scale lacustrine fan-delta sedimentary model suitable for the Baikouquan Formation in the study area (Fig. 11). Under a humid climate, abundant rainwater was responsible for the migration of sediments out of the valley and accumulation at the mountain pass and nose-shaped platform area to form fan-delta plain deposition. Debris flow formed near the mountain pass and the river channel during the flash flood

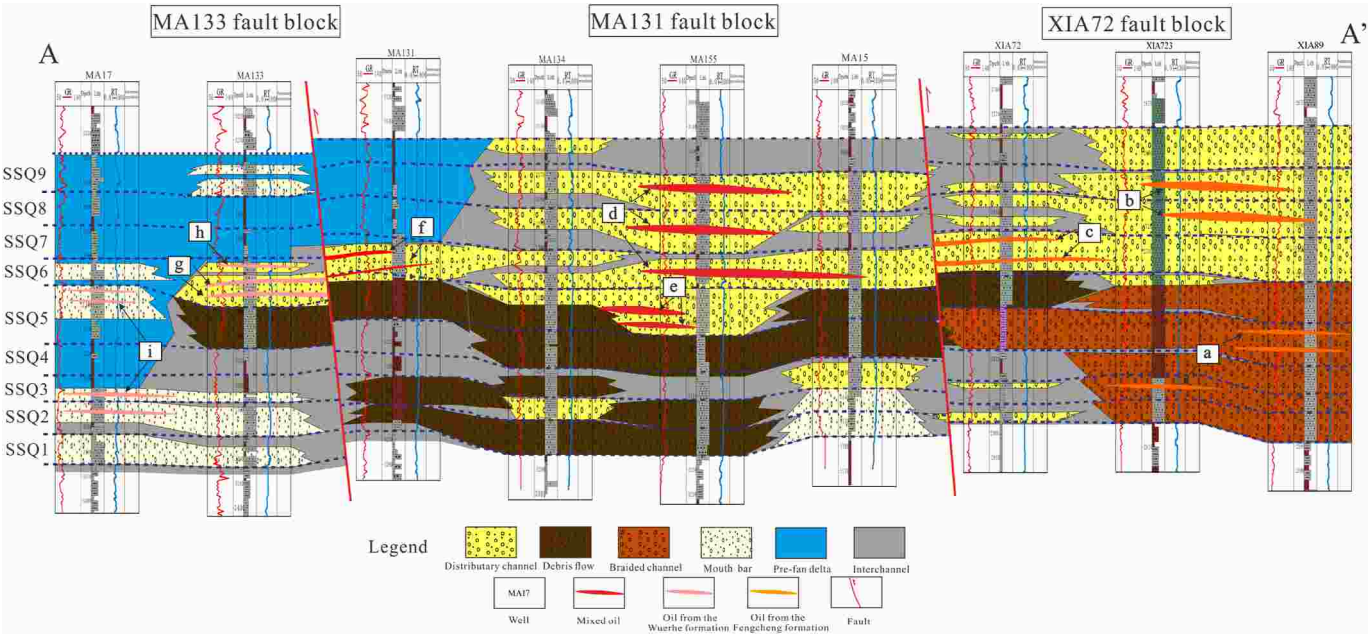

Fig. 10. Vertical distribution of the hydrocarbon reservoir model in different fault blocks. (a) lithologic hydrocarbon reservoir model with braided river sand bodies and oil from P_1f, (b) lithologic hydrocarbon reservoir model with distributary channel sand bodies and oil from P_1f, (c) fault-lithologic hydrocarbon reservoir model with distributary channel sand bodies and oil from P_1f, (d) lithologic hydrocarbon reservoir model with distributary channel sand bodies and mixed oil, (e) laterally screened hydrocarbon reservoir model with distributary channel sand bodies and mixed oil, (f) fault-lithologic hydrocarbon reservoir model with distributary channel sand bodies and mixed oil, (g) fault-lithologic hydrocarbon reservoir model with distributary channel sand bodies and oil from P_2w, (h) lithologic hydrocarbon reservoir model with distributary channel sand bodies and oil from P_2w, and (i) lenticular lithologic hydrocarbon reservoir model with mouth bar sand bodies and oil from P_2w.

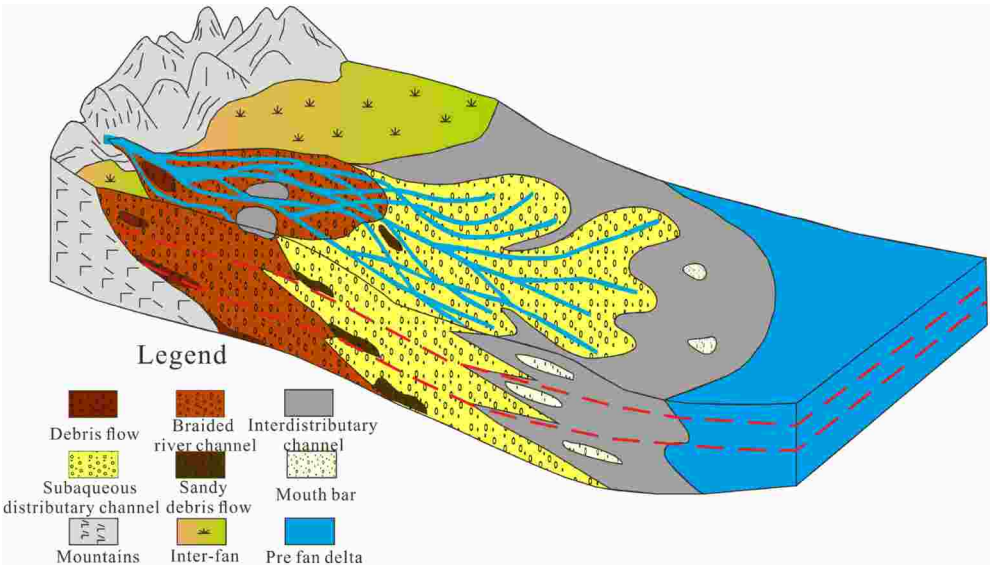

Fig. 11. Depositional model of the lacustrine fan delta of the Baikouquan Formation in the study area.

period. Braided channels generally developed in the trenches during the late flood period and the constant flow period, where traction flow sand bodies were deposited. During the constant flow period, the sedimentary deposits carried by the river entered the lake basin through the braided channel on the slope of the fan delta, forming subaqueous distributary channels in the fan-delta front. The strong hydrodynamic force created by abundant water and the slope potential energy made the subaqueous distributary channels extend further, thus fully elutriating and transporting the gravels to form sand bodies with low argillaceous content. From bottom to top, the fan delta in the Baikouquan Formation gradually retrograded toward the mountain direction. Moreover, the sand bodies of mouth bars transformed and migrated in the waves and coastal currents in the lake basin.

5.2. Controls on the hydrocarbon accumulation

Hydrocarbon migration channels in this area were the deep faults, sand bodies, and regional unconformities between the Permian and the Triassic. Deep faults connected to the Fengcheng Formation provide a vertical channel for upward hydrocarbon migration, whereas sand bodies and unconformities serve as channels for lateral adjustment and migration of hydrocarbon generated from the Wuerhe Formation. A considerably decreased crude oil density in each fault block was observed as the burial depth became shallower, suggesting the migration of hydrocarbon from the lower position to the structural highs. The hydrocarbon reservoir models of the lacustrine fan delta complex are jointly controlled by a combination of different types of faults and reservoirs. However, there are considerable differences in the degree to which oil and gas enrichment has occurred among the different types of hydrocarbon reservoirs. Based on the production data in the wells, the oil and gas enrichment of the hydrocarbon reservoirs in the fan-delta front is apparently better than that in the fan-delta plain in the north and the mouth bars in the south.

Although fault blocks and the fan-delta front microfacies considerably control the hydrocarbon accumulation, the reservoir quality variation inside the fan-delta front is considered a primary factor controlling hydrocarbon accumulation. Casting thin-section observation and core sample physical properties have shown that the muddy content of the Baikouquan Formation is negatively correlated with reservoir porosity and permeability (Fig. 12). The porosity decreases from 13% to 7% with increasing muddy content from 1% to 7% (Fig. 13a), but there is an abrupt decrease in permeability of more than two orders of magnitude

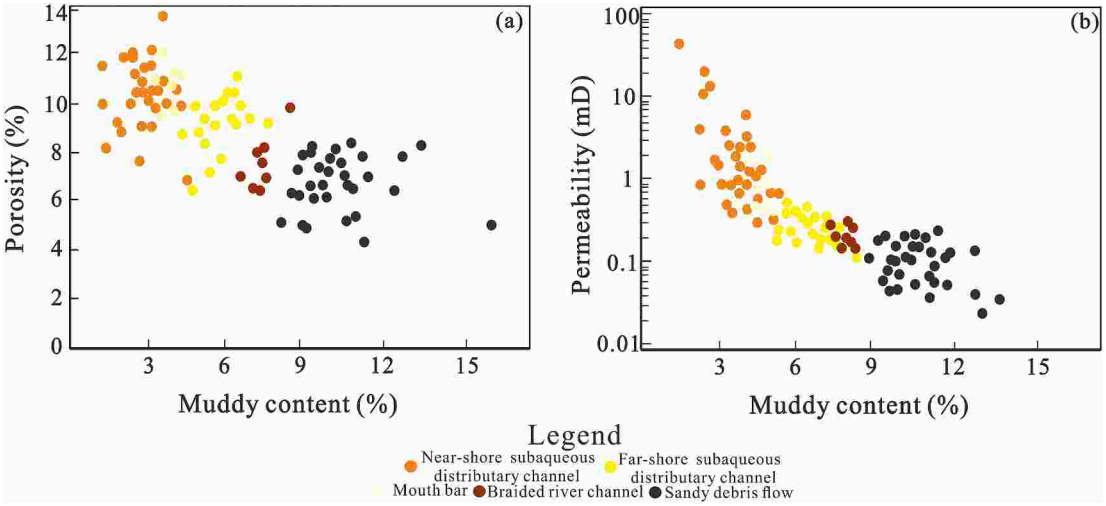

Fig. 12. Crossplots between muddy content and physical properties: (a) muddy content versus porosity; (b) muddy content versus permeability.

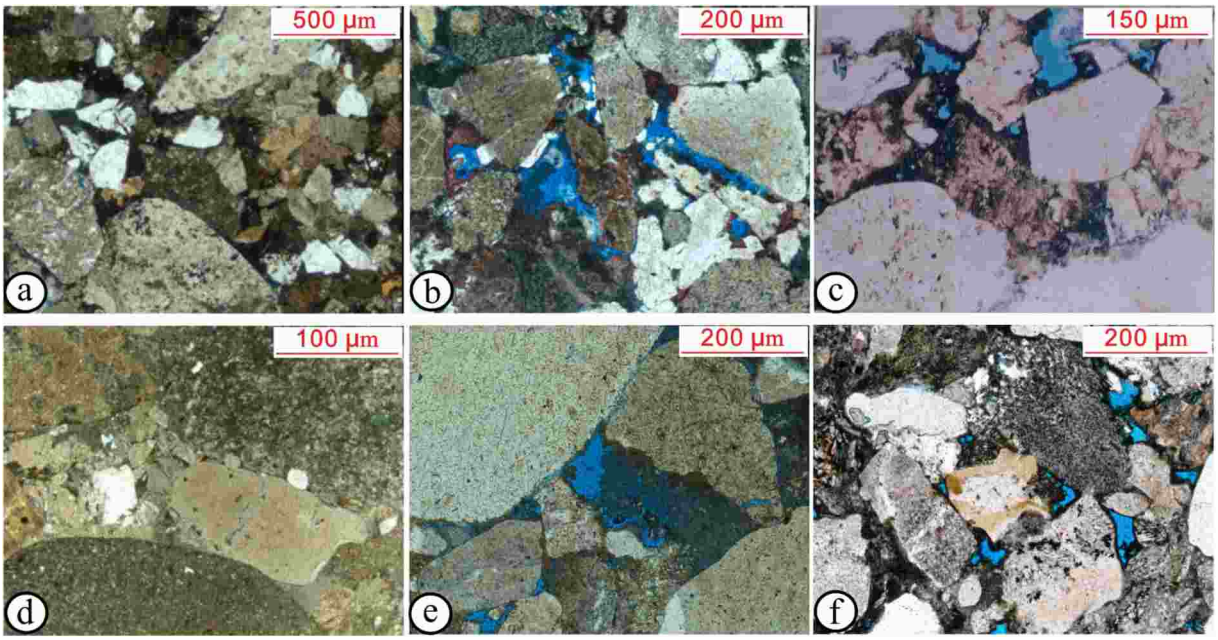

Fig. 13. Physical properties by thin-section analysis. (a) Sandy conglomerate with a muddy content of 7.5%, few pores can be observed, Φ: 4.5%, K: 0.51 mD, well XIA89, 2505.77 m, plane-polarized light (PPL). (b) Sandy conglomerate with a muddy content of 2.0%, residual intergranular pores are developed, Φ: 11.9%, K: 3.49 mD, well XIA89, 2477.27 m, PPL. (c) Conglomeratic coarse sandstone, intergranular pores are exhibited, Φ: 13.1%, K: 2.65 mD, well MA133, 3302.14 m, PPL. (d) Medium-grained conglomerate, pores are observed in microfractures, Φ: 5.0%, K: 0.19 mD, well XIA89, 2504.70 m, PPL. (e) Fine-grained conglomerate, intergranular pores are developed, Φ: 12.8%, K: 7.61 mD, well MA15, 3088.20 m, PPL. (f) Gravelly coarse sandstone, intergranular pores are developed, Φ: 12.2% ; K: 2.87 mD, well MA13, 3107.64 m, PPL. Φ denotes the porosity, K denotes the permeability.

(from 32 to 0.2 mD) (Fig. 13b), that is, the seepage capacity of the reservoir is severely reduced by the presence of argillaceous matrix residues in the pore throat. Apart from the muddy content, the variation in grain size arising from sediment gravity differentiation is an important factor in determining the reservoir quality. Core observation indicates that the lithology of the Baikouquan Formation reservoir in the study area comprises sandy fine conglomerate, medium conglomerate, and gravelly (medium) coarse sandstone. Under the identical sedimentary microfacies, the reservoir grain size is correlated with physical properties. By comprehensive analysis of the core, thin section, particle size, and mercury injection data, the order of reservoir quality is gravelly (medium) coarse sandstone > fine conglomerate > medium conglomerate (Fig. 13c, d, e, f). Gravelly (medium) coarse sandstone refers to the reservoir with a porosity exceeding 12%, whereas medium conglomerate corresponds to the reservoir with porosity less than 7%. In conclusion, two periods of hydrocarbon charging have occurred in the petroleum system and different fault blocks are characterized by distinct categories of crude oil and enormous hydrocarbon is transported and accumulated in the fan-delta front reservoir with low muddy content and fine grain size.

5.3. Implications for petroleum exploration

The oil and gas enrichment of the fan delta complex in the Baikouquan Formation is influenced by hydrocarbon accumulation and reservoir quality. Hydrocarbon charging between the three fault blocks of the research region exhibits considerable variability during the deposition of the Baikouquan Formation. The deep faults and unconformity between the Permian and the Triassic of the Mahu Sag are crucial in controlling the migration pathways of hydrocarbon accumulation, which has afforded distinct oil and gas types and enrichment degree of large, lacustrine fan delta systems. Conversely, the nearshore, fan-delta front with a fine-grain size and low muddy content is considered an excellent reservoir offering good hydrocarbon leads and possible prospects.

Apart from geological conditions, attention should be paid to some engineering factors. For tight conglomerate reservoir development, rational exploitation with natural energy is adopted for oil yielding and formation pressure is highly correlated with its production capacity. The hydrocarbon generation period associated with the effective source rocks in the high-formation pressure area lasted longer than that in the normal-pressure area, thereby continuously forming mature-to-high mature oil and gas. Furthermore, high pressure has a positive effect for the preservation of the pore system and enhancement of reservoir physical properties by blocking the discharge pathway of pore water, decreasing the effective stress of the reservoir, and weakening the compaction degree. Overall, the pore structure of such a reservoir is characterized by medium-to-low porosity, micro-to-fine throat, and poor seepage capacity. Large-scale fracturing is the premise and an effective approach to improving seepage capacity and productivity. However, the formation of a complex fracture network via reservoir fracturing requires favorable stress-field conditions and rock fabric characteristics with smaller discrepancy between the minimum and maximum horizontal stresses, developed natural fractures, and higher brittleness index. In contrast to a shale reservoir, coarse-grained conglomerate has distinct mechanical properties and fracturing mechanism. Future work on reservoir development must focus on considering the parameter, which is the main controlling factor of fracturing to enhance the EUR of a single well for the production development of tight oil reservoirs.

6. Conclusions

The Triassic in the northern Mahu Sag comprises five third-order sequences, whereas the Baikouquan Formation is a third-order sequence at the bottom of the Triassic. The medium-term fifth-order sequence boundaries were determined via the geophysical logging responses and core samples, which were used for constructing a high-resolution sequence stratigraphic framework. Therefore, there were nine fifth-order sequences in the Baikouquan Formation (SSQ1–SSQ9) in

the wells. Owing to multistage lake transgressions and regressions, the sandy conglomerate was predominantly enriched in the fifth-order sequences SSQ1–SSQ6 and SSQ8, whereas mudstone mainly developed in SSQ7 and SSQ9.

Fan-delta plain, fan-delta front, and prefan-delta sedimentary subfacies successively developed in the fan delta complex. Furthermore, eight microfacies have been identified via detailed core observation, among which sandy debris flow and subaqueous distributary channels dominate, accounting for ~80% of the depositional system. Subsequently, stratal slices were employed to produce seismic facies maps within an isochronous sequence stratigraphic framework, which could reveal the sedimentary evolution of the fan delta's progradation and retrogradation in the Baikouquan Formation. In conclusion, the northern Xiazijie and eastern Madong fan delta systems were determined. The northern Xiazijie fan delta showed a wide distribution area with interactive progradation and retrogradation during SSQ1–SSQ6 sequences, whereas for SSQ7–SSQ9, the Xiazijie fan delta gradually underwent complete retrogradation. The eastern Madong fan delta system only developed during SSQ1–SSQ5 under abrupt paleotopographic slope break.

Two hydrocarbon charging periods were observed in the fan delta reservoir of the Baikouquan Formation. The hydrocarbon migration channels in this area were the deep faults, sand bodies, and regional unconformities between the Permian and the Triassic. Fault blocks have a considerable influence on hydrocarbon charging, where physical properties of crude oil, formation pressure, and saturation degree have distinct characteristics. Based on source rocks, faults, and reservoirs, hydrocarbon reservoir models of the study area are divided into nice categories. The oil and gas enrichment of the hydrocarbon reservoirs is influenced by different factors in the three fault blocks. Deep faults and unconformities between the Permian and the Triassic of the Mahu Sag are crucial in controlling the migration pathways of hydrocarbon accumulation. The fan-delta front microfacies considerably control the hydrocarbon accumulation, whereas the reservoir quality variation inside the fan-delta front within fine grain size and low muddy content is a vital factor in controlling hydrocarbon accumulation. In addition, engineering factors, such as formation pressure, the discrepancy between the minimum and maximum horizontal stresses, natural fractures, and brittleness index, are jointly correlated with the production capacity of tight conglomerate reservoirs.

Author contribution

Zhichao Yu: Conceptualization, Methodology, Writing-original draft, Writing-review, and editing. Zhizhang Wang: Project administration and Supervision. Jie Wang: Formal analysis. Ziyan Li: Formal analysis.

Declaration of competing interest

The authors declare that they have no known competing financial interests or personal relationships that could have appeared to influence the work reported in this paper.

Acknowledgements

This study was supported by the Strategic Cooperation Technology Projects of CNPC and CUPB (Grant No. ZLZX2020-01). We are deeply grateful to the Exploration and Development Research Institute of Xinjiang Oilfield, CNPC, for providing research data and publication permission. We thank the Editor and anonymous reviewers for their thorough and critical reviews as well as suggestions, which have considerably improved the quality of this manuscript.

References

Amy, L.A., 2019. A review of producing fields inferred to have upslope stratigraphically trapped turbidite reservoirs: trapping styles (pure and combined), pinch-out formation, and depositional setting. AAPG (Am. Assoc. Pet. Geol.) Bull. 103 (12), 2861–2889.

Anyiam, U.O., Uzuegbu, E., 2020. 3D seismic attribute-assisted stratigraphic framework and depositional setting characterization of frontier Miocene to Pliocene aged Agbada Formation reservoirs, deep offshore Niger Delta Basin. Mar. Petrol. Geol. 122.

Carll, J.F., 1880. The geology of theoil regions of Warren, Ven-ango, and Butler counties. In: The 2nd Pennsylvania Geol Survey, 3, pp. 481–482.

Feng, Chong, Lei, Dewen, Qu, Jianhua, Huo, Junzhou, 2019. Controls of paleo-overpressure, faults and sedimentary facies on the distribution of the high pressure and high production oil pools in the lower Triassic Baikouquan Formation of the Mahu Sag, Junggar Basin, China. J. Petrol. Sci. Eng. 176, 232–248. https://doi.org/10.1016/j.petrol.2019.01.012.

Ehman, K.D., et al., 2021. Miocene seismic stratigraphy and geomorphology of Bibiyana gas field, Surma Basin, Bangladesh. AAPG (Am. Assoc. Pet. Geol.) Bull. 105 (9), 2317–2347.

Dai, Jinxing, Yunyan, N.I., Liu, Quanyou, Wu, Xiaoqi, Gong, Deyu, Feng, H.O.N.G., Zhang, Yanling, Fengrong, L.I.A.O., Zengmin, Y.A.N., Hongwei, L.I., 2021. Sichuan super gas basin in southwest China. Petrol. Explor. Dev. 48 (6), 1251–1259. https://doi.org/10.1016/S1876-3804(21)60284-7.

Li, Wandi, Luo, Dongkun, Yuan, Jiehui, 2017. A new approach for the comprehensive grading of petroleum reserves in China: two natural gas examples. Energy 118, 914–926. https://doi.org/10.1016/j.energy.2016.10.125.

Liang, Yuanyuan, Zhang, Yuanyuan, Chen, Shi, Guo, Zhaojie, Tang, Wenbin, 2020. Controls of a strike-slip fault system on the tectonic inversion of the Mahu depression at the northwestern margin of the Junggar Basin, NW China. J. Asian Earth Sci. 198, 104229. https://doi.org/10.1016/j.jseaes.2020.104229.

Lu, Xinchuan, Sun, Dong, Xie, Xiangyang, Chen, Xin, Zhang, Shuncun, Zhang, Shengyin, Sun, Guoqiang, Shi, Ji'an, 2019. Microfacies characteristics and reservoir potential of triassic Baikouquan Formation, northern Mahu sag, Junggar Basin, NW China. J. Nat. Gas Geosci. 4 (1), 47–62. https://doi.org/10.1016/j.jnggs.2019.03.001.

Melo, A.H., et al., 2021. High-resolution sequence stratigraphy applied for the improvement of hydrocarbon production and reserves: a case study in Cretaceous fluvial deposits of the Potiguar basin, northeast Brazil. Mar. Petrol. Geol. 130.

Pan, J., et al., 2021. Origin and charging histories of diagenetic traps in the Junggar Basin. AAPG (Am. Assoc. Pet. Geol.) Bull. 105 (2), 275–307.

Bahmani, Ali Asghar, Riahi, Mohammad Ali, Ramin, Nikrouz, 2020. Detection of stratigraphic traps in the Asmari Formation using seismic attributes, petrophysical logs, and geological data in an oil field in the Zagros basin, Iran. J. Petrol. Sci. Eng. 194, 107517. https://doi.org/10.1016/j.petrol.2020.107517.

Shang, W., et al., 2022. High-resolution sequence stratigraphy in continental lacustrine basin: a case of eocene Shahejie Formation in the Dongying depression, Bohai bay basin. Mar. Petrol. Geol. 136.

Song, Xianqiang, Meng, Lingdong, Fu, Xiaofei, Wang, Haixue, Sun, Yonghe, Jiang, Wenya, 2020. Sealing capacity evolution of trap-bounding faults in sand-clay sequences: insights from present and paleo-oil entrapment in fault-bounded traps in the Qinan area, Bohai Bay Basin, China. Mar. Petrol. Geol. 122, 104680. https://doi.org/10.1016/j.marpetgeo.2020.104680.

Tang, Wenbin, Zhang, Yuanyuan, Pe-Piper, Georgia, 2021. Permian to early Triassic tectono-sedimentary evolution of the Mahu sag, Junggar Basin, western China: sedimentological implications of the transition from rifting to tectonic inversion. Mar. Petrol. Geol. 123, 104730. https://doi.org/10.1016/j.marpetgeo.2020.104730.

Tian, Jingchun, Liang, Qingshao, Wang, Feng, Li, Jian, Yu, Wei, Chen, Weizhen, 2022. Sedimentary records of seismic events in a lacustrine basin of continental depression: a case study of the Triassic Yanchang Formation in the Ordos Basin, Northern China. J. Asian Earth Sci. 228, 105128. https://doi.org/10.1016/j.jseaes.2022.105128.

Vail, P.R., 1987. Seismic stratigraphy interpretation using sequence stratigraphy. Part 1: seismic stratigraphy interpretation procedure. In: Bally, A.W. (Ed.), Atlas of Seismic Stratigraphy, vol. 27. American Association of Petroleum Geologists, Studies in Geology, pp. 1–10.

Warnecke, M., Aigner, T., 2019. Influence of subtle paleo-tectonics on facies and reservoir distribution in epeiric carbonates: integrating stratigraphic analysis and modelling (U. Muschelkalk, SW Germany). Sediment. Geol. 383, 82–100. https://doi.org/10.1016/j.sedgeo.2019.01.015.

Wu, W., et al., 2020. Seismic sedimentology, facies analyses, and high-quality reservoir predictions in fan deltas: a case study of the Triassic Baikouquan Formation on the western slope of the Mahu Sag in China's Junggar Basin. Mar. Petrol. Geol. 120.

Xian, B., et al., 2018. Using of stratal slicing in delineating delta-turbidite systems in Eocene Dongying depression, Bohai Bay Basin: insights for the evolution of multi-source delta-turbidite systems in a fourth order sequence. J. Petrol. Sci. Eng. 168, 495–506.

Xiao, Zhenglu, Chen, Shijia, Liu, Chaowei, Lu, Zixing, 2021. lake basin evolution from early to middle Permian and origin of triassic Baikouquan oil in the western margin of Mahu sag, Junggar Basin, China: evidence from geochemistry. J. Petrol. Sci. Eng. 203, 108612. https://doi.org/10.1016/j.petrol.2021.108612.

Xu, Zhaohui, Hu, Suyun, Wang, Lu, Zhao, Wenzhi, Cao, Zhenglin, Wang, Ruiju, Shi, Shuyuan, Jiang, Lei, 2019. Seismic sedimentologic study of facies and reservoir

in middle triassic Karamay Formation of the Mahu sag, Junggar Basin, China. Mar. Petrol. Geol. 107, 222–236. https://doi.org/10.1016/j.marpetgeo.2019.05.012.
Yu, Zhichao, Wang, Zhizhang, et al., 2021. Volcanic lithology identification based on parameter-optimized GBDT algorithm: a case study in the Jilin Oilfield, Songliao Basin, NE China. J. Appl. Geophys. 194, 104443. https://doi.org/10.1016/j.jappgeo.2021.104443.
Zhao, Wenzhi, Suyun, H.U., Xujie, G.U.O., 2019. New concepts for deepening hydrocarbon exploration and their application effects in the Junggar Basin, NW China. Petrol. Explor. Dev. 46 (5), 856–865. https://doi.org/10.1016/S1876-3804(19)60245-4.
Zhu, Rukai, Zou, Caineng, Mao, Zhiguo, Yang, Haibo, Xiao, Hui, Wu, Songtao, Cui, Jingwei, 2019. Characteristics and distribution of continental tight oil in China. J. Asian Earth Sci. 178, 37–51. https://doi.org/10.1016/j.jseaes.2018.07.020.